STScI | SPACE TELESCOPE SCIENCE INSTITUTE

Instrument Science Report COS 2018-08(v1)

The Spatial Resolution of the COS FUV channel at Lifetime Position 4

Andrew Fox[1]

[1] Space Telescope Science Institute, 3700 San Martin Drive, Baltimore, MD 21218

16 February 2018

ABSTRACT In this ISR we report on the COS FUV spatial resolution at Lifetime Position 4 (LP4), as determined via analysis of the cross-dispersion spread functions (XDSFs). The XDSFs are predicted by the Code V optical model of the COS system and validated via high-S/N observations taken at LP4. We present analysis of the XDSFs in multiple central wavelength settings of the three COS FUV gratings: G130M, G160M, and G140L, deriving the dependence of the width (FWHM) of the XDSFs vs. wavelength. We find good agreement (RMS$<$1 pixel) between the predictions and the models on the FUVB segment, but in several settings the data are broader than the models by 1–2 pixels on FUVA.

Contents

1. Introduction

On October 2, 2017, routine operations of the COS FUV channel were moved to a new Lifetime Position, LP4. This date was chosen to coincide with the start of Cycle 25. All Cycle 25 COS/FUV observations are now executed by default at LP4, with the exception of the blue modes (G130M/1055 and G130M/1096) that remain at LP2. The move to LP4 was made in order to mitigate the effect of gain sag and provide the community with access to an unsagged region of the FUV detector. LP4 is located 5.0 arcseconds below LP1 in the cross-dispersion direction, and 2.5 arcseconds below LP3. The move to LP4 was accompanied by a new set of restrictions on detector segment usage, FP-POS settings, and target acquisition settings, that together are known as the COS2025 policies, described at http://www.stsci.edu/hst/cos/cos2025.

The change in FUV lifetime position incurs a change in spatial resolution as well as spectral resolution. The spatial resolution is described quantitatively by the cross-dispersion spread functions (XDSFs), which encode the spatial distribution of flux from a point source in the y-direction on the FUV detector, just as the line spread functions (LSFs) encode the distribution in the dispersion (x) direction. The XDSFs can be predicted by optical models (see Section 3) and measured in observational data taken at LP4 (see Section 4), and the predictions and observations can be directly compared. In this ISR, we report on such a comparison. For comparison, the *spectral* resolution analysis at LP4 is presented in a separate ISR (Fox et al. 2018).

The analysis described in this ISR broadly follows the spatial resolution analysis at LP2 presented by Roman-Duval et al. (2013). Further information on the XD profiles at LP4 is contained in the PROFTAB and TRACETAB reference files used by the `calcos` pipeline, and the generation of these files is described in Rafelski et al. (2018).

2. Observations

A log of observations for the COS data analyzed in this ISR is given in Table 1. They were taken under two programs: 14842 (PI=P. Sonnentrucker; 1291 and 1327 cenwaves) and 15366 (PI=A. Fox; 1222, 1577, and 1623 cenwaves). The target in both programs is AzV75, a blue supergiant star in the Small Magellanic Cloud with spectral type O5.5I(f), chosen for two main reasons: (1) it is UV-bright but not too bright for COS, so high signal-to-noise ratios (S/N=60) can be reached relatively quickly without exceeding the count rate limits for the FUV detector; (2) it is heavily reddened, with $E(B-V)$=0.16, ensuring a high foreground neutral gas column N(H I), which in turn allows many narrow interstellar metal lines to be detected in absorption. As such the spectrum is rich in narrow features whose width can be analyzed as an indicator of the spectral resolution. Program 14842 was executed in summer 2016 as part of the LP4 exploratory phase, whereas Program 15366 was executed in summer 2017 in the LP4 calibration phase. Both datasets are similar in their S/N properties, with S/N=60 per resolution element when combined over the four FP-POS positions.

Setting	Prog. ID	Date (UT)	Exposure Time[a] (s)	Dataset ID
G130M/1222	15366	2017-08-10	1552	ldm701010
G130M/1291	14842	2016-08-29	800	ldb301020
G130M/1327	14842	2016-08-29	800	ldb301040
G160M/1577	15366	2017-08-10	2070	ldm701020
G160M/1623	15366	2017-08-10	2070	ldm701030

Table 1. Log of observations for LP4 resolution programs.
[a] Total exposure time combined across FP-POS position.

3. Code V Optical Models

We examine model predictions for the LP4 spatial resolution generated from the Code V optical code, which uses an optical model of the COS system provided by Tom Delker (Ball Aerospace) and updated by Erin Elliott on 4/2/2017. The advantage of Code V over ray-trace codes is that it properly characterizes the wings of the COS LSF, which contain a significant fraction of the total power in the profile. The profiles are known to be non-gaussian due to mid-frequency wavefront errors, which are due to polishing errors on the primary and secondary *HST* mirrors (Ghavamian et al. 2009).

Full details on the focus position at LP4 and its impact on the Code V models are given in Fox et al. (2018). The models are used to generate line spread functions (LSFs; dispersion direction) and cross-dispersion spread functions (XDSFs) as a function of wavelength for each cenwave. The LSFs and XDSFs are computed as a function of pixel number, and are each normalized such that their integral is equal to one.

4. Spatial Resolution Determination

We derive the FWHM of the XDSFs in the observed data at LP4 as a function of cenwave and wavelength. To form the XDSFs, we take the calibrated 2-D images produced by the `calcos` pipeline (*flt_a.fits and *flt_b.fits files). We collapse the data in the x-direction in regions $\pm$2Å in width around each wavelength, and then extract the profile in the y-direction. Because the profiles are non-Gaussian, we measure their actual FWHM (i.e. we identify the width of the normalized profile at height 0.5) rather than by fitting the profile with Gaussian components. We compare these observed FWHMs with the predictions from the Code V models in Figure 1. Note that while all thirteen LP4 cenwaves are included in the models (six from G130M, five from G160M, two from G140L) only five cenwaves have observational data, as described in Table 1. Airglow regions around Lyman-α and O I λ1302 are excluded from the analysis.

Figure 1 shows good agreement (in the FWHM of the XDSF) between the Code V models and observations for the 1327 and 1623 cenwaves, but some disagreement on the FUVA segment for 1222 and 1291 (caused by undulations in the observed FWHM), and substantial disagreement for the FUVA segment of 1577. To further explore these

differences, we computed the residuals in pixels (in the sense data–model) in the XDSF FWHM as a function of wavelength, for each cenwave. These residuals are shown in Figure 2, where we annotate the RMS residual for FUVB and FUVA for each setting. They are formed by interpolating the model FWHM array onto the (rebinned) wavelength array in the data. This figure shows that the Code V model reproduces the observed FWHM closely for the 1327, 1577, and 1623 settings. 1291 shows more structure, with the data slightly narrower than the model on FUVB but slightly broader on FUVA.

The final set of figures we show is Figure 3 where we plot the actual shape of the XDSF profiles (for both data and models) at six reference wavelengths for each cenwave. The reference wavelengths chosen span both the FUVA and FUVB detector segments in each case. Clear non-Gaussianity of the XDSF is seen in these profiles, with a strong dependence on wavelength, though it also depends on grating. For G130M, the asymmetry becomes more pronounced at low wavelength, where a broad "shoulder" is present in the line profiles, offset by $\approx$+20 pixels from the primary peak. This shoulder is strongest in the 1222 setting. For G160M, the profiles are narrower than with G130M, with only minor asymmetries (similarly, G160M has the best spectral resolution of the three FUV gratings). For G140L, the profiles are most symmetric near the center of the bandpass, but become asymmetric to high and low wavelength, with a prominent shoulder developing at +10–20 pixels in the y-direction in both cases.

5. Conclusions

In this ISR we have presented an analysis of the spatial resolution of the COS FUV detector at LP4, using a comparison of predicted XDSFs from the Code V optical model with on-orbit observations. The Code V XDSFs have been validated for the G130M/1222, G130M/1291, G130M/1327, G160M/1577, and G160M/1623 cenwaves. This was accomplished by:
(1) extracting the FWHM of the XDSFs as a function of wavelength for each Code V model, and comparing them with the actual FWHMs measured in LP4 data. Agreement is found at the sub-pixel level on segment FUVB, and at the 1–2 pixel level on FUVB, where the data tends to be broader than the models.
(2) analyzing the (non-Gaussian) shape of the XDSFs for each cenwave in the analysis, to compare the XD profile between the models and the data. The data confirm the model prediction that the XDSFs become more non-Gaussian at low wavelength.

Change History for COS ISR 2018-08

Version 1: 16 February 2018- Original Document

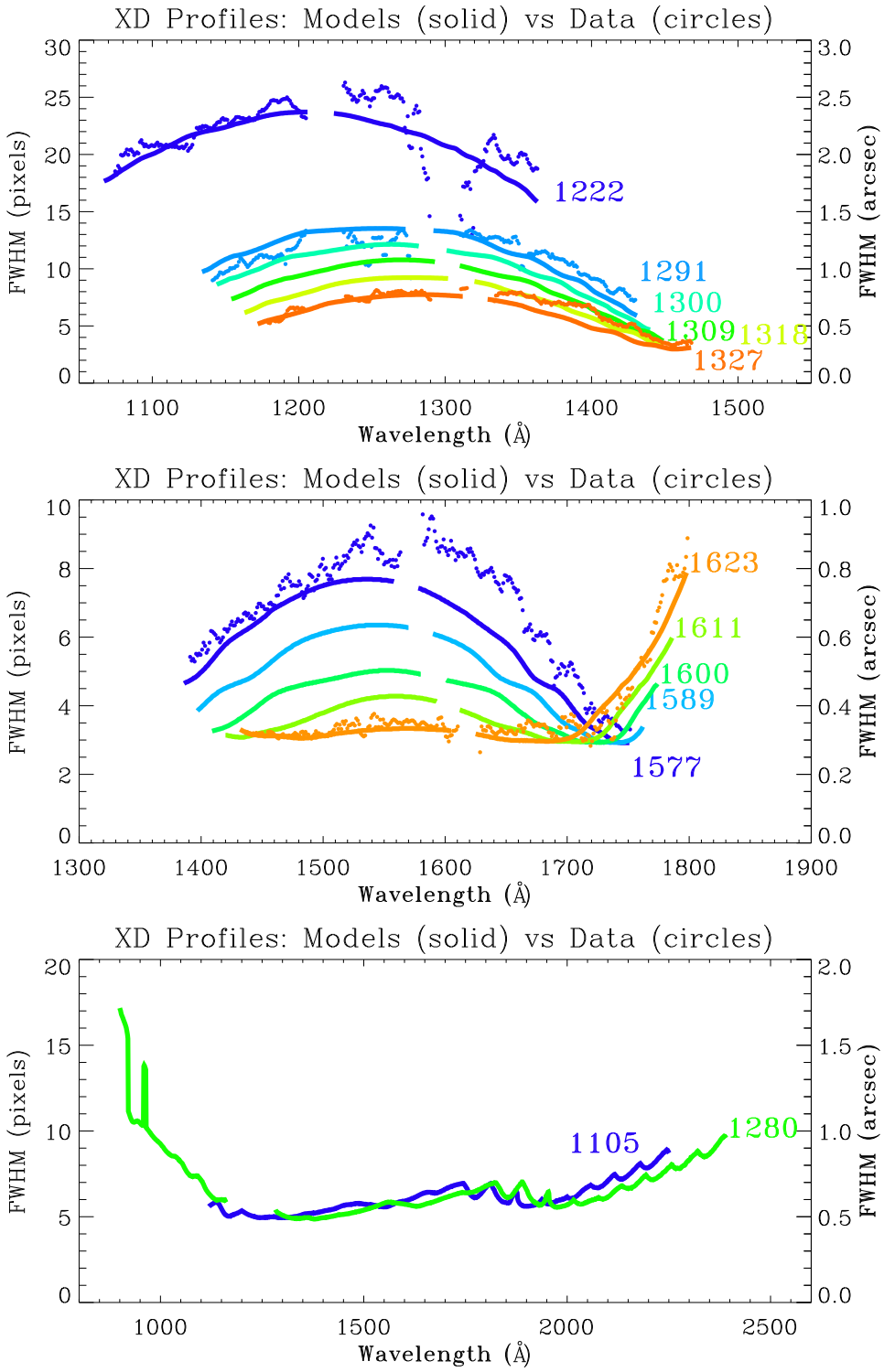

Figure 1. FWHM of the cross-dispersion profiles (XDSFs) as a function of wavelength for G130M, G160M, and G140L cenwaves at LP4. The solid curves show the predictions from the Code V model. The colored dots show the observed profiles at LP4 (for the five settings where they exist). The y-axis on the right shows the FWHM in arcseconds using a plate scale of 0.10 arcsec per pixel.

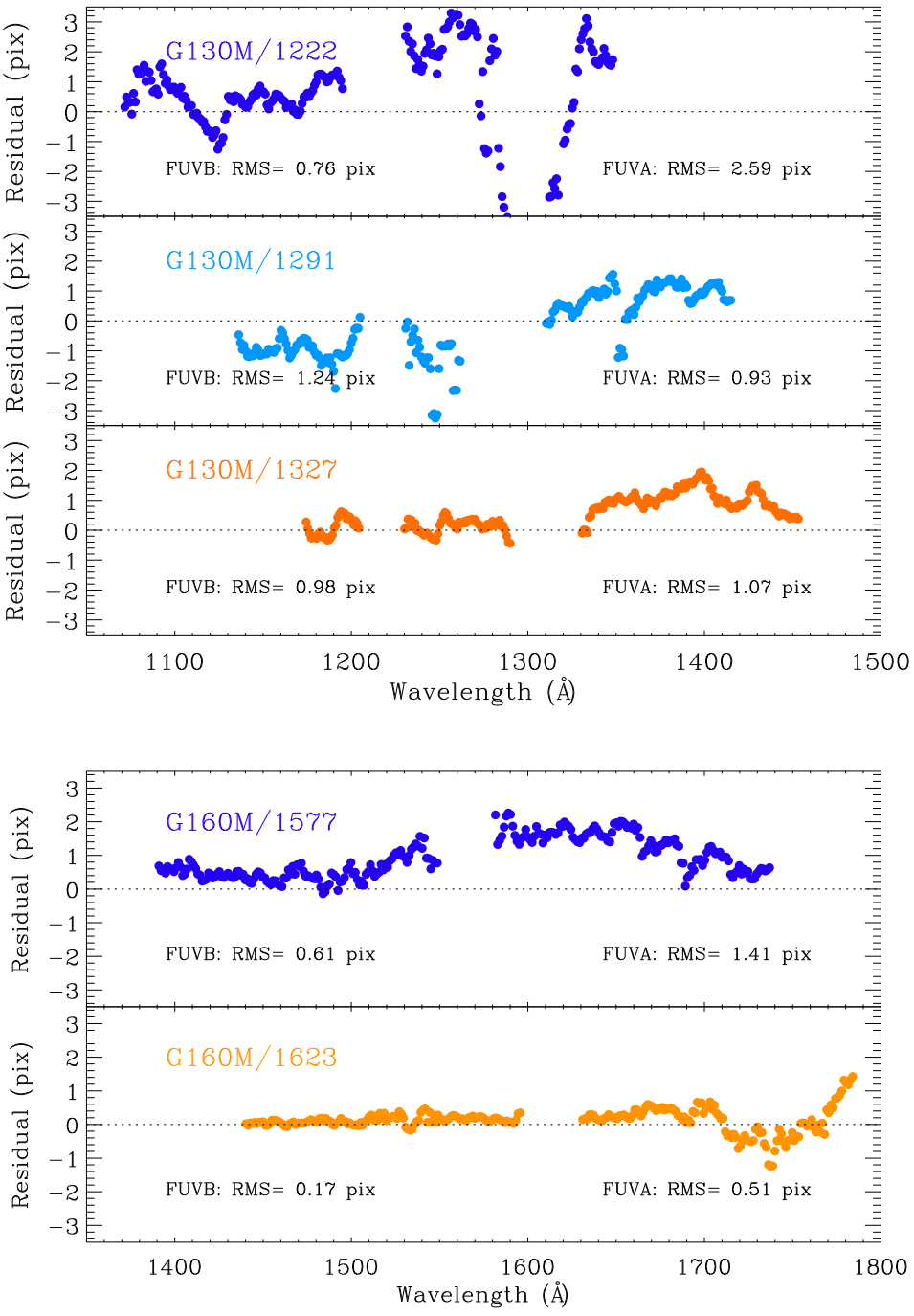

Figure 2. Residuals in pixels between data and models for the width (FWHM) of the XDSFs vs. wavelength. The top three panels show the G130M settings. The lower two show the G160M settings. The RMS residual in the detector segments is annotated on each panel.

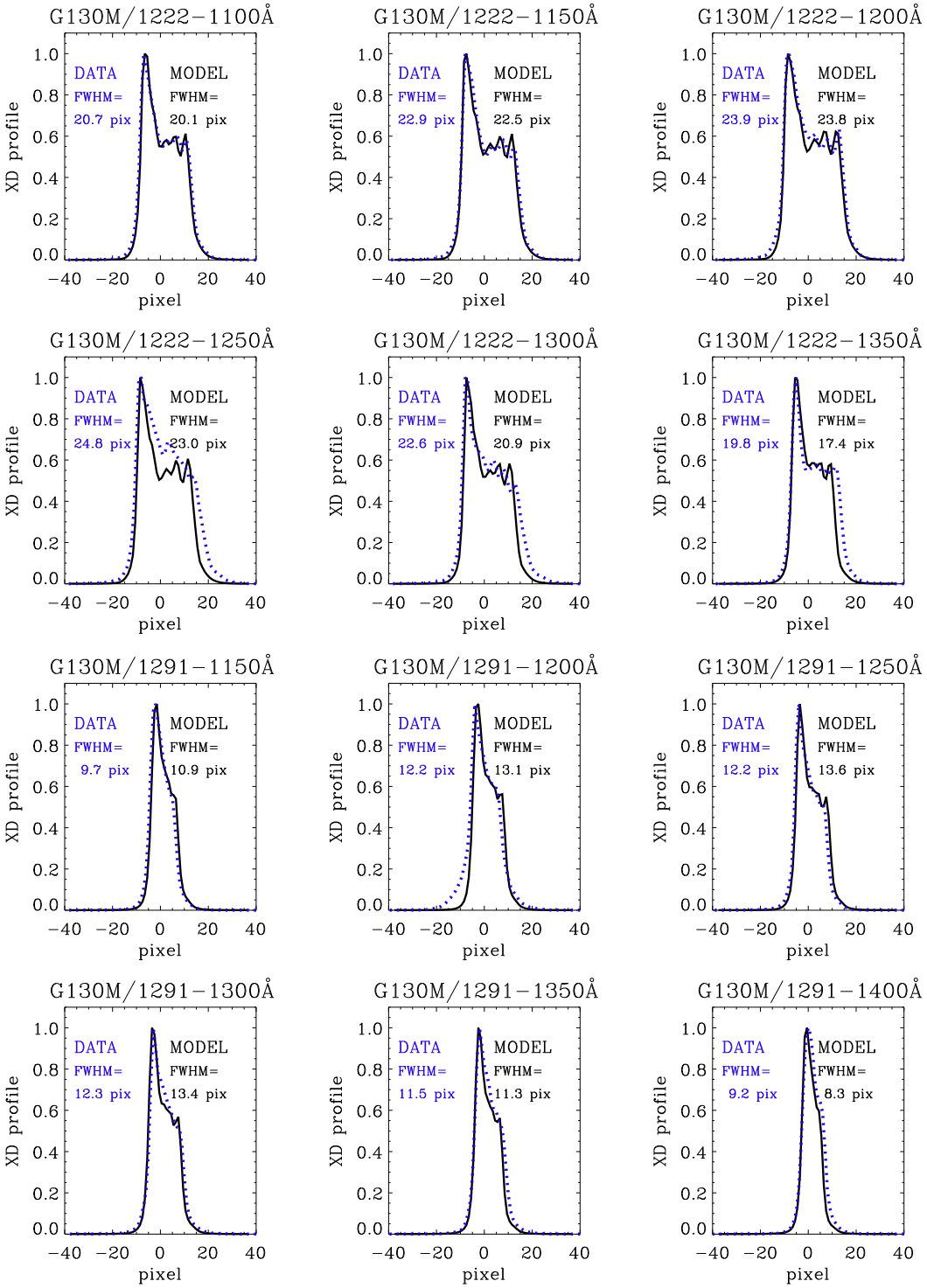

Figure 3. Cross-dispersion profiles at LP4 at six different reference wavelengths for two G130M cenwaves: 1222 (top) and 1291 (bottom). In each case the solid black lines show the Code V predictions and the dashed blue lines show the observations at LP4. The measured FWHMs are annotated on the panel for both data and models.

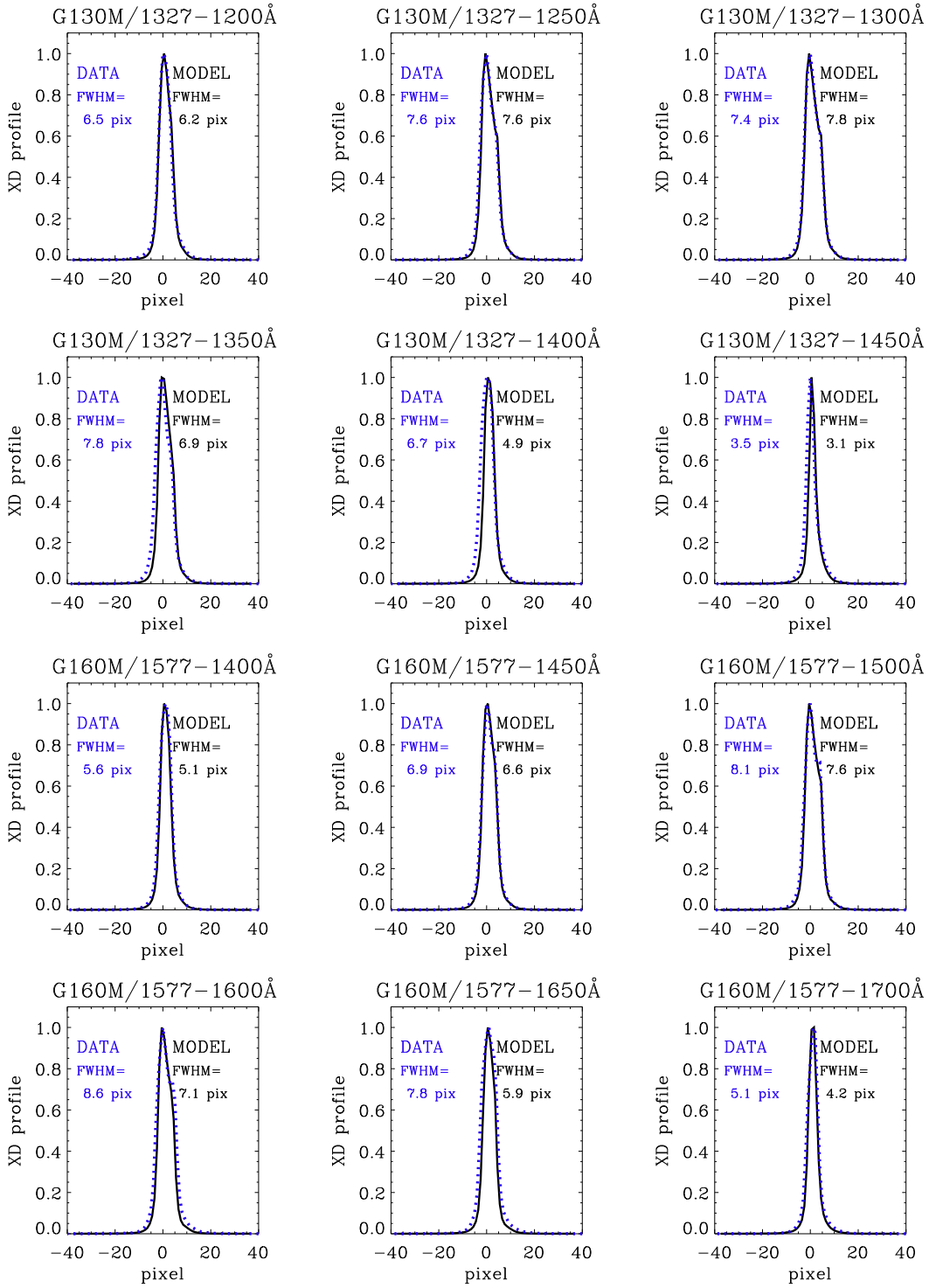

Figure 3. (cont.) Cross-dispersion profiles for G130M/1327 (top) and G160M/1577 (bottom).

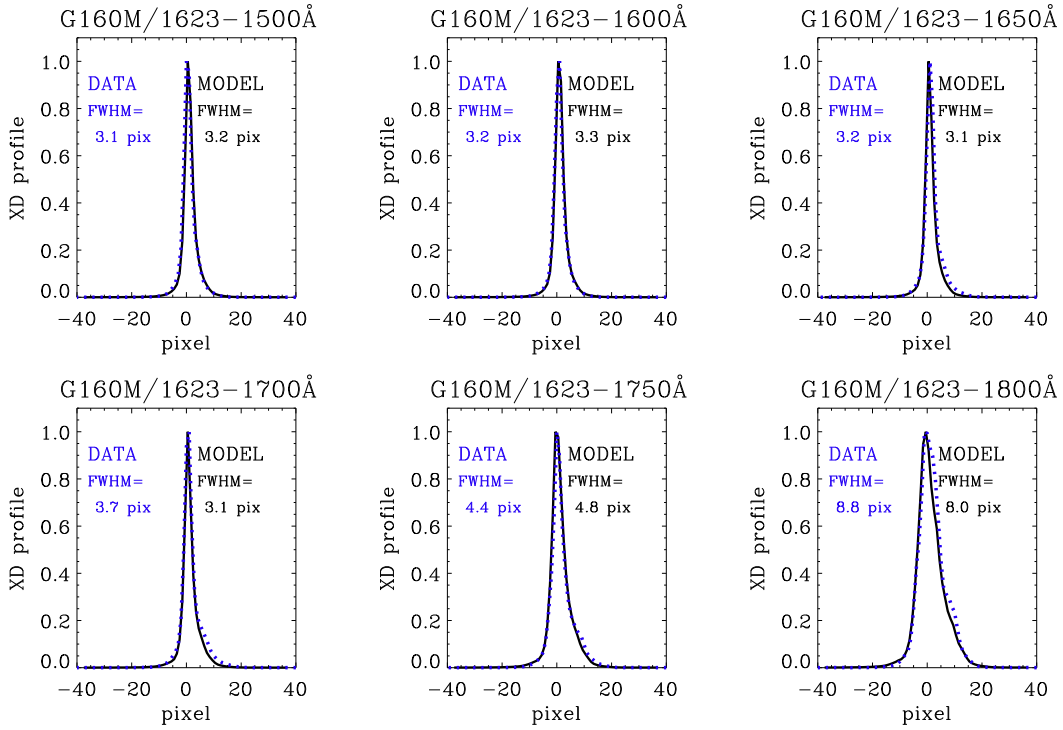

Figure 3. (cont.) Cross-dispersion profiles for G160M/1623.

References

Fox, A., et al. 2017, Instrument Science Report COS 2017-17
Focusing the COS/FUV G160M and G130M Gratings at Lifetime Position 4
Fox, A., et al. 2018, Instrument Science Report COS 2018-07
The Spectral Resolution of the COS FUV channel at Lifetime Position 4
Ghavamian, P., et al. 2009, Instrument Science Report COS 2009-01
Preliminary Characterization of the Post-Launch Line Spread Function of COS
Rafelski, M., et al. 2018, Instrument Science Report in prep
Profiles and Traces at COS FUV Lifetime Position 4
Roman-Duval, J., et al., 2013, Instrument Science Report COS 2013-07,
COS/FUV Spatial and Spectral Resolution at the new Lifetime Position
Sonnentrucker, P., et al., 2017a, Instrument Science Report COS 2017-16
FUV Focus Sweep Exploratory Program for COS at LP4
Sonnentrucker, P., et al., 2017b, Instrument Science Report COS 2017-20,
Quick-check of the COS/FUV G130M Spectral Resolution at Lifetime Position 4

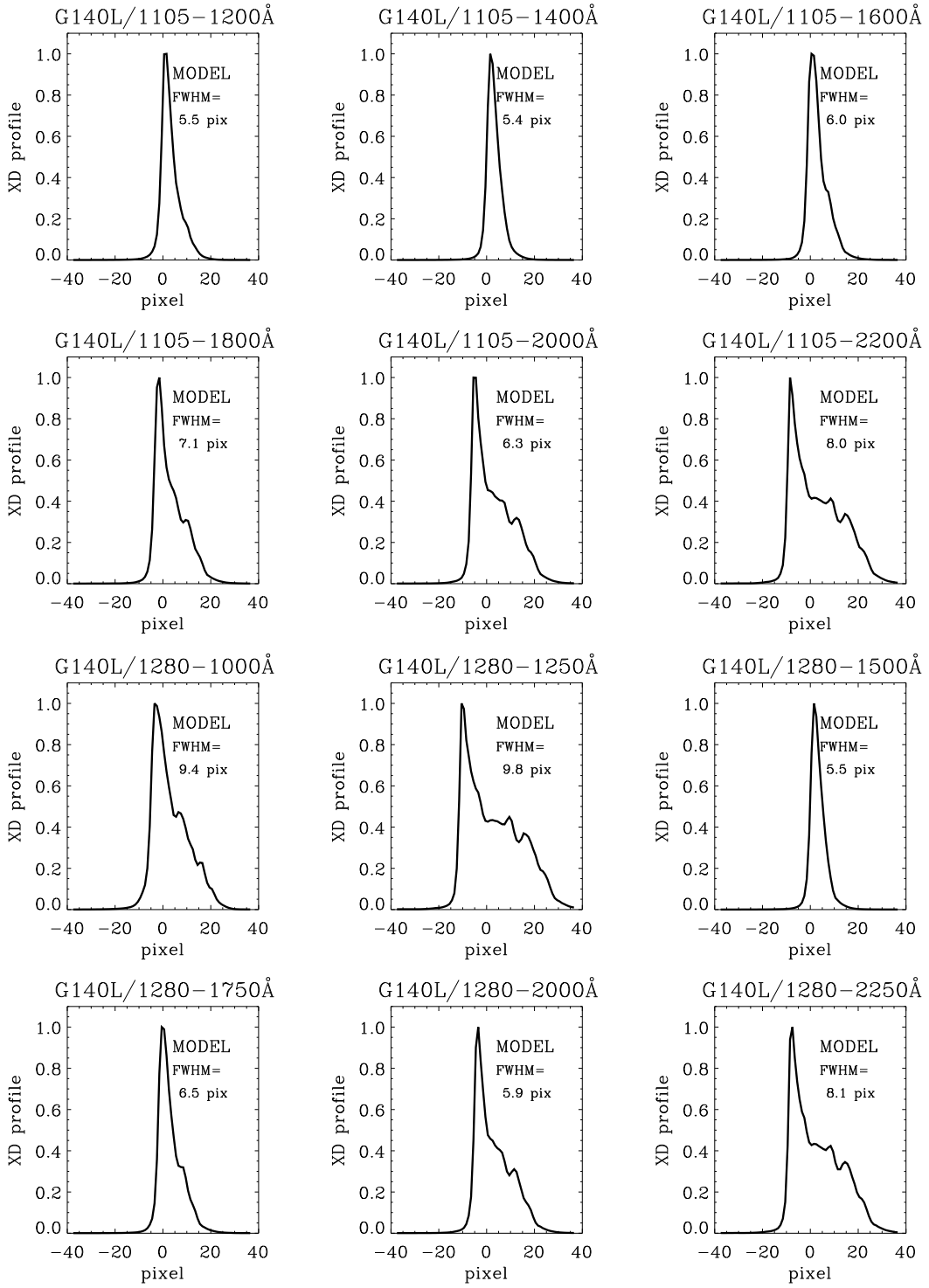

Figure 3. (cont.) Cross-dispersion profiles for G140L/1105 (top) and G140L/1280 (bottom). No data are available for these settings so only models are shown.